

Dynamic Responses and Wake Characteristics of a Floating Offshore Wind Turbine in Yawed Conditions

Shun Xu¹, Xiaoming Zhang², Weiwen Zhao¹, Decheng Wan^{1*}

¹ Computational Marine Hydrodynamic Lab (CMHL), School of Naval Architecture, Ocean and Civil Engineering, Shanghai Jiao Tong University, Shanghai, China

² Zhongnan Engineering Corporation Limited, Changsha, China

*Corresponding author

ABSTRACT

A coupled large eddy simulation and aero-hydro-moor-servo dynamics code is used to perform numerical simulations of a floating offshore wind turbine (FOWT) under yawed conditions. The atmospheric boundary layer wind field is simulated by large eddy simulation (LES) with sufficient simulation duration as the inflow wind condition. Two cases with 15° and 30° yaw angles of wind turbine are performed, and the results of aerodynamics, hydrodynamics and wake characteristics are compared and analyzed with that of non-yaw scenario. It is concluded that the rotor power of FOWT decreases with increase of yaw angle, whereas the rotor thrust of 15° yaw angle is slightly larger than that of non-yaw situation. There is no distinct difference of platform surge motion and pitch motion between the 15° yaw angle and non-yaw scenario, whereas the two motions of 30° yaw angle are significantly less than that of non-yaw scenario. The platform sway motion increases with the increase of yaw angle due to the crosswise component of rotor thrust of wind turbine. What's more, faster wake recovery and more significant wake deflection with increase of yaw angle is observed, which is beneficial for the inflow wind condition and power generation of downstream wind turbine.

KEY WORDS: Floating offshore wind turbine; Yawed conditions; Large eddy simulation; Aero-hydrodynamics; Wake characteristics.

INTRODUCTION

In recent years, the wind energy has become a hot topic due to its advantages of non-pollution, renewable and rich resources (Rohrig et al., 2019). The wind energy harvesting consists of two parts: onshore and offshore. Compared to onshore wind energy, the offshore wind energy resources are more abundant, and without the limitations of land space and noise (Li et al., 2020). In addition, the most of wind energy resources are distributed in deep water area, i.e., more than 80% of offshore wind resources are available in sea area with depth > 60 m. The bottom-fixed offshore wind turbine is not suitable for deep water scenario, because the construction cost of bottom foundation will increase dramatically with the increase of water depth, which is commercially expensive and impractical. One possible solution is to change the fixed foundation to floating foundation. Consequently, in order to harvest the wind resources

in deep water area and ensure it is commercially feasible, the design and development of floating offshore wind turbine (FOWT) becomes an attractive work (Ramachandran et al., 2022).

In contrast to prototype and scale-down basin experiment, the numerical simulation of FOWT is cheaper for the cost, and the computational cost is more affordable with the significant advancement of high-performance computer. Therefore, the numerical simulation becomes a powerful and indispensable tool for the design and development of FOWT. In order to yield accurate analysis results and support the design of FOWT, Tran and Kim (2016) proposed a high-fidelity computational model using overset mesh technique. The numerical results of unsteady aerodynamics, platform hydrodynamic responses and mooring tension forces showed a good agreement with the test data and numerical results calculated by NREL FAST code. Zhang and Kim (2018) also performed high-fidelity numerical analysis of a semi-submersible FOWT by using overset mesh technique in commercial software STAR CCM+. Their results revealed that the rotor thrust of FOWT is increased by 7.8% compared to that of onshore wind turbine, whereas the rotor power is decreased by 10%.

For the numerical analysis of FOWT, the high-fidelity overset mesh technique is computationally expensive and time consuming (Xu et al., 2022), which limits its further application in numerical investigation of FOWT. Trolborg et al. (2007) pointed out that the actuator line model (ALM) used for wind turbine aerodynamics can improve the computational efficiency by representing the wind turbine as body force, and the accuracy of results can be guaranteed by solving the Navier-Stokes equations. Consequently, Cheng et al. (2019) developed an aero-hydrodynamic model of FOWT namely FOWT-UALM-SJTU based on the combination of the ALM and an in-house two-phase CFD solver. In order to reflect the unsteady aerodynamics of FOWT, an additional velocity induced by the motions of floating platform was modified into the conventional ALM. Huang and Wan (2019) presented a systematic study on the interaction between wind turbine and floating platform by using the validated and verified FOWT solver FOWT-UALM-SJTU, and they noted that the local angle of attack is significantly altered by surge and pitch motions of floating platform. After that, Huang et al. (2021) developed an aero-hydro-elastic numerical framework of FOWT. The elastic ALM is proposed to predict the blade deformation of FOWT based on the integration between the ALM considering additional velocity induced by platform motions and the one-dimensional finite element method structure model.

Among the above numerical studies of FOWT, the inflow wind condition

is simplified, i.e., the uniform wind inflow and shear wind inflow. However, the FOWT is operated in atmospheric boundary layer (ABL) wind field, in which the wind inflow is definitely turbulent. With the increase of wind turbine diameter, the effects of turbulence wind on aerodynamic performance of FOWT are more significant. Therefore, Li et al. (2018) investigated the effects of ABL wind field on the aerodynamics of a FOWT, and their results demonstrated that the power generation of FOWT is sensitive to the ABL wind field. Zhou et al. (2022) explored the influence of inflow wind condition on aerodynamics and platform motions of a semi-submersible FOWT. Three inflow wind conditions were employed in their work, specifically, the turbulent wind inflow, shear wind inflow and uniform wind inflow. What's more, Doubrawa et al. (2019) investigated the fatigue loads of a spar-type FOWT under ABL wind fields. The turbulent wind fields were generated by large eddy simulations and synthetic turbulent wind model, and the results based on different turbulent wind generation methods were compared and analyzed.

In addition to the high turbulence, another significant feature of the ABL wind field is non-stationary (Porté-Agel et al., 2020), in which the change of wind direction is very frequent. Consequently, the yaw operation of FOWT is a common situation. However, most of the numerical studies of FOWT are concentrated on the non-yaw scenario, specifically, the wind direction is perpendicular to the rotation plane of wind turbine. When the inflow wind direction changes, the aerodynamic performance, platform hydrodynamic responses and wake characteristics are significantly changed. Therefore, the dynamic responses of the yawed FOWT requires more attention to be systematically investigated. In this study, we present the numerical investigations of a yawed FOWT immersed in the ABL wind fields by using a coupled LES and aero-hydro-moor-servo dynamics code. We employ the LES with sufficient simulation duration to simulate the ABL turbulent wind inflow. The ALM is applied to predict the aerodynamic performance and wake characteristics of FOWT, and the coupled dynamic responses of FOWT is simulated and predicted by NREL FAST code. The numerical results of aerodynamic performance, platform motions and wake characteristics of FOWT with different yaw angles are compared and analyzed with the non-yaw scenario.

NUMERICAL METHODS

Governing Equations

In order to better simulate the turbulence in ABL wind field and analyze the characteristics in wind turbine wake, the LES is used for the simulations of ABL wind field and FOWT. The spatial filtered governing equations including continuity equation and momentum equation are presented as follows:

$$\frac{\partial \bar{u}_i}{\partial x_i} = 0 \quad (1)$$

$$\frac{\partial \bar{u}_i}{\partial t} + \frac{\partial}{\partial x_j} (\bar{u}_j \bar{u}_i) = - \underbrace{\frac{\partial \bar{p}}{\partial x_i}}_I - \underbrace{\frac{1}{\rho_0} \frac{\partial}{\partial x_i} \bar{p}_0(x, y)}_{II} - \underbrace{2\varepsilon_{ijk} \Omega_3 \bar{u}_k}_{III} - \underbrace{\frac{\partial}{\partial x_j} (\tau_{ij}^D)}_{IV} + \underbrace{\frac{1}{\rho_0} f_i^T}_V \quad (2)$$

where, the overbar denotes the spatial filtered value, subscript $i = 1, 2, 3$ are the components of a variable of x-, y- and z-axis, respectively, in the right side of momentum equation, Term I is the modified pressure gradient, the modified pressure \bar{p} consists of two parts, the resolved pressure subtracting the background driving pressure normalized by ρ and one third of the stress tensor trace, i.e., $\bar{p} = (\bar{p} - p_0 + \rho g z) / \rho + \tau_{kk} / 3$; Term II is the background pressure gradient, which is used to drive the wind field to a desired wind speed at specified height; Term III

is the Coriolis force, reflecting the influence of earth rotation on ABL wind field; Term IV is the tensor of fluid stress induced by the turbulence model of LES, the Smagorinsky sub-scale model (Smagorinsky, 1963) is used to calculate the stress and closure the momentum equation; Term V is a source term of body force of wind turbine blade, which is needed when the wind turbine is introduced into the wind field and used to consider the effect of wind turbine on flow field. Note that the viscous stress is neglected because of the high Reynolds-number feature of the ABL wind field. More details of the governing equations can be obtained in this reference (Churchfield et al., 2021a).

Actuator Line Model

Different from the blade-resolved overset mesh technique, the wind turbine modeled by ALM can significantly save the computational cost, while the numerical accuracy is guaranteed by solving the governing equations of flow field. The ALM was originally proposed by Sorensen and Shen (2002), and the ideal behind this method is to regard the wind turbine as body force in flow field. The wind turbine blades are divided into many blade elements along the radial direction of blade, and the blade element theory is used to calculate the aerodynamic force of each blade element. In order to consider the disturbance of wind turbine on flow field, the forces of blade elements are imposed on flow field by adding a source term of body force to the momentum equation. Figure 1 shows an analysis of velocity vectors of a two-dimensional airfoil. The relative inflow velocity U_{rel} is determined by:

$$U_{rel} = \sqrt{U_z^2 + (\Omega r - U_\theta)^2} \quad (3)$$

where, U_z is the axial component of inflow wind velocity; U_θ is the tangential component of inflow wind velocity; Ω is the rotor speed; r is the radial distance from blade element to rotor center.

The aerodynamic force of a blade element is calculated by:

$$f = (L, D) = \frac{1}{2} \rho U_{rel}^2 c dr (C_L \bar{e}_L + C_D \bar{e}_D) \quad (4)$$

where, L and D are the lift and drag forces of blade element, respectively; ρ is the air density; c is the chord length of two-dimensional airfoil; dr is the width of blade element; C_L and C_D are the coefficients of lift and drag forces; \bar{e}_L and \bar{e}_D are the unit vectors of lift and drag forces.

The coefficients of lift and drag forces are determined by local angle of attack α , which is equal to the difference between local angle of inflow ϕ and local angle of pitch γ . The local angle of inflow ϕ is determined by inflow wind condition.

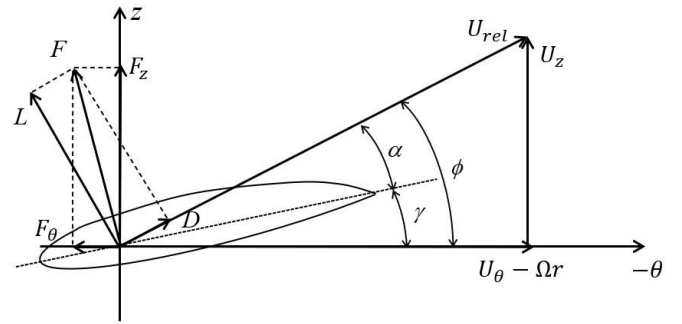


Figure 1. Velocity vectors of a two-dimensional airfoil.

The numerical singularity occurs when the aerodynamic forces of blade elements are directly imposed on flow field. Therefore, we use the Gauss kernel function to smooth the body force of wind turbine imposed on flow field. The smooth body force is expressed by:

$$f_\varepsilon = f \otimes \eta_\varepsilon = \sum_{i=1}^N f_i(x_i, y_i, z_i, t) \frac{1}{\varepsilon^3 \pi^{\frac{3}{2}}} \exp \left[- \left(\frac{d_i}{\varepsilon} \right)^2 \right] \quad (5)$$

where, N is the number of blade elements of a turbine blade; (x_i, y_i, z_i) is the position of i -th blade element; d_i is the distance between the blade element and projection position; ε is the projection width, $\varepsilon \approx 2\Delta x$ (Troldborg, 2009) is recommended to ensure numerical stability; Δx is the mesh size near blade element.

Simulation Procedure

A coupled LES and aero-hydro-moor-servo dynamics of FOWT code is used in this work, which is proposed and implemented in NREL SOWFA framework (Churchfield et al., 2012b), a LES solver for numerical simulations of large wind farm based on open-source OpenFOAM CFD framework (Jasak et al., 2007). The simulation procedure of a yawed FOWT immersed in ABL wind field is shown in Figure 2. Firstly, the LES with sufficient simulation duration (18600s) is used to develop the quasi-equilibrium ABL wind field. The data of last 600s of a plane is saved as the inflow wind condition for the simulations of the yawed FOWT. The wind turbine blades are modeled by the ALM and the wake is simulated in LES framework. The fully coupled aero-hydro-moor-servo dynamics of FOWT are simulated and predicted by NREL FAST code (Jonkman and Buhl, 2005) (version 8.16). The coupling between LES framework and FAST code is implemented by delivering the wind velocity on blade element solved by CFD and the position of blade element solved by FAST code to each other. Note that the coupling between LES framework and FAST code is developed and proposed by NREL SOWFA, not in this work. This coupled code has been widely used for the simulations of wind turbine under ABL inflow (Johlas et al., 2021; Chanprasert et al., 2022). Due to the wind velocity on blade element is solved by the ALM in LES framework, the momentum part of blade element momentum theory is neglected in FAST code for wind turbine aerodynamics. What's more, the numerical methods about the aero-hydro-moor-servo dynamics of FOWT are not presented, because a baseline and built-in case of FOWT in FAST is adopted in this work, we believe the numerical methods of FOWT used in FAST can be easily found in its theory guide (NREL, 2022).

of yaw operation on dynamic responses and wake characteristics of FOWT, the yaw controller module in FAST is inactive.



Figure 3. Overview of the FOWT model.

Table 1. Gross properties of NREL 5MW wind turbine.

Term	Value
Rated power	5 MW
Rated wind velocity	11.4 m/s
Rated rotor velocity	12.1 rpm
Hub height	90 m
Orientation	Upwind
Blade number	3

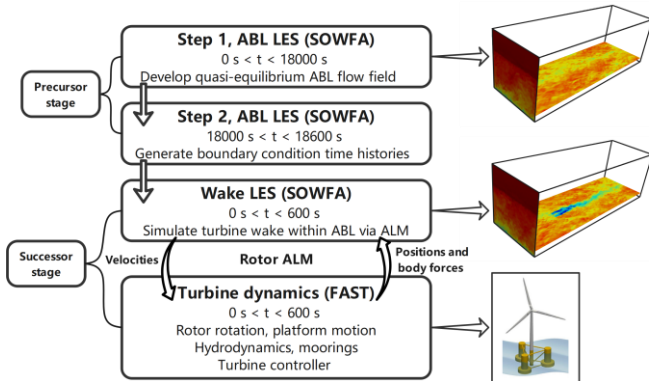


Figure 2. Simulation procedure of FOWT immersed in ABL wind field.

SIMULATION CASES

Wind turbine model

The NREL 5MW wind turbine (Jonkman et al., 2009) mounted on OC4 semi-submersible floating platform (Robertson et al., 2014) is used as the FOWT model, as shown in Figure 3. The wind turbine is a conventional upwind wind turbine with three blades. The gross properties are summarized in Table 1. There are three controllers available for this wind turbine: torque controller, blade pitch controller and yaw controller. Due to the aim of this work is to investigate the effect

The OC4 DeepCwind semi-submersible floating platform is adopted to support the wind turbine. The floating platform is composed of three main offset columns, one central column and some diagonal cross and horizontal bracing components. In order to limit the hydrodynamic responses of floating platform, a mooring system including three mooring lines are used. The offset angle between two adjacent mooring lines is 120° , as shown in Figure 4. Note that only the wind turbine is in yaw operation, the orientation of floating platform and mooring system is not changed, i.e., the initial configuration of mooring line #2 is aligned with the inflow direction of combined wind-wave. The overall parameters of floating platform and mooring system are concluded in Table 2.

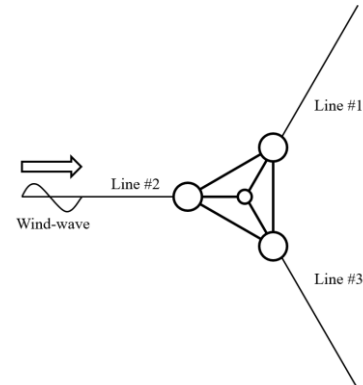


Figure 4. Orientation of floating platform and mooring system.

Table 2. Gross properties of floating platform and mooring system.

Term	Value
Draft	20 m
Platform mass	13,473,000 kg
Displacement	13,986.8 m ³
Centre of mass	(0 m, 0 m, -13.5 m)
Platform roll inertia	6.827×10 ⁹ kg·m ²
Platform pitch inertia	6.827×10 ⁹ kg·m ²
Platform yaw inertia	1.226×10 ¹⁰ kg·m ²
Depth to anchor	200 m
Depth to fairlead	14 m
Mooring line diameter	0.0766 m
Equivalent line mass density	113.35 kg/m
Equivalent mooring line extensional stiffness	753.6 MN

Simulation of ABL wind field

The ABL wind field is simulated by the LES with sufficient simulation duration. The computational domain of simulation of ABL wind field is a hexahedron, in which the length, width and height of this domain is 3000m, 1000m and 1000m, respectively, as shown in Figure 5. The mesh resolution is the same in the whole domain, i.e., 10m × 10m × 10m in x-, y- and z-axis, and the corresponding mesh number is 3 million. The cyclic boundary is employed on the four vertical boundaries, which denoting that the wind field at downstream will re-enter the upstream. The top boundary is a slip boundary, reflecting that there is no vertical velocity gradient at this height level. A wall stress model of Schumann (Schumann, 1975) is used on bottom boundary to calculate the surface stress, in which the surface roughness is 0.001 to represent a typical sea surface condition. The initial wind condition is uniform wind with velocity of 11.4m/s in the whole domain, including the boundaries. The simulation time is 18600s to generate the quasi-equilibrium ABL wind field, and the time step is 0.2s. The data of last 600s of upstream boundary plane is saved as the inflow condition of the FOWT.

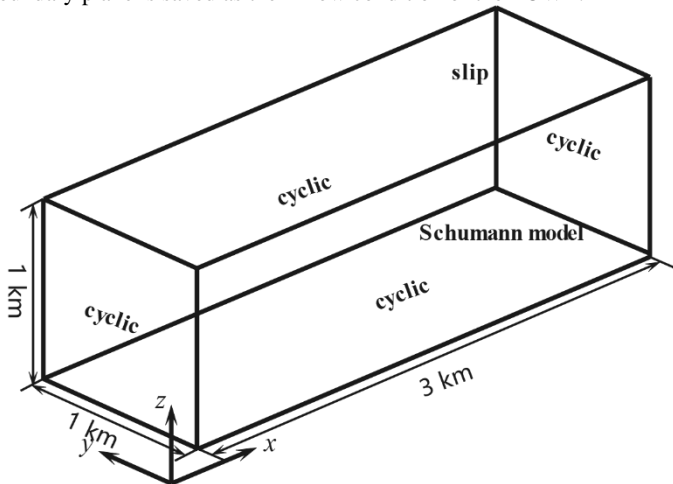


Figure 5. Computational domain and boundary conditions of simulation of ABL wind field.

Simulation of FOWT

The computational domain and background mesh resolution of simulation of FOWT in LES framework are the same as that of simulation of ABL wind field, i.e., 3km × 1km × 1km and 10m × 10m × 10m. Figure 6 shows the computational domain and mesh refinement of simulation of FOWT. The wind turbine is positioned at

downstream 800m of upstream inflow boundary, which is denoted by black line. In order to capture the vortices in wind turbine wakes, we employ a two-level mesh refinement of hexahedral region. The length, width and height of first-level refinement region are 13D, 4D and 3D, respectively, and D=126m is the rotor diameter. The distance between wind turbine and upstream boundary of first-level refinement region is 3D. The size of first-level refinement region is reduced by 2D, 1D and 1D inward in three directions respectively, which is the second-level refinement region. After the mesh refinement, the mesh resolution near wind turbine is 2.5m × 2.5m × 2.5m, and the total mesh number is 12 million.

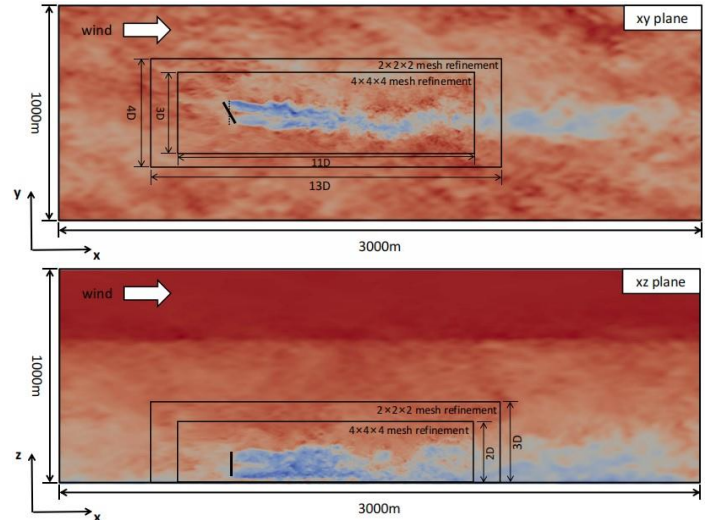


Figure 6. Computational domain and mesh refinement of simulation of FOWT.

In comparison to the boundary conditions of ABL wind field, the upstream inflow boundary of simulation of FOWT is changed to mapping boundary condition, indicating that the time histories of data saved in ABL wind field are used as the inflow condition of simulation of FOWT. What's more, zero gradient condition is applied on downstream boundary to allow the flow field to out freely. The flow field of wind turbine simulation is initialized by the ABL wind field at time instant of 18000s. The simulation time of FOWT is 600s, and the time step is 0.02s to limit the blade tip to advance more than one grid at one time step. In the result analysis, we exclude the first 200s data of numerical results to eliminate the influence of transient startup of wind turbine.

The fully coupled aero-hydro-moor-servo dynamics of FOWT is simulated and predicted by NREL FAST code. Note that the wind velocity of FOWT is solved and sampled in the LES framework, therefore, the momentum part of blade element momentum theory used in AeroDyn module is replaced by the ALM, and the InflowWind module used for generation of inflow wind condition is inactive. The simulation time in FAST is 600s, but the time step is 0.005s, which means one time step of LES framework contains four-time iterations of FAST simulation.

For the combined wind-wave condition of FOWT, the simulated wind field in LES framework is used, in which the mean wind speed profile is shear and the wind speed at hub height is 11.4m/s, and the time-averaged characteristics of inflow wind are presented and analyzed in following section. The Stokes first-order regular wave with wave height of 7.58m and period of 12.1s is employed as the incident wave condition. Two yaw angles of 15° and 30° of wind turbine are adopted, and the results are compared to that of non-yaw scenario, therefore, we name the three cases as $\theta_{yaw} = 0^\circ$, $\theta_{yaw} = 15^\circ$ and $\theta_{yaw} = 30^\circ$. It is noteworthy again

that only the wind turbine is in yaw operation, the orientation of floating platform and mooring system is consistent with that of non-yaw scenario, i.e., the initial configuration of mooring line #2 is aligned with the inflow direction of combined wind-wave, as shown in Figure 4.

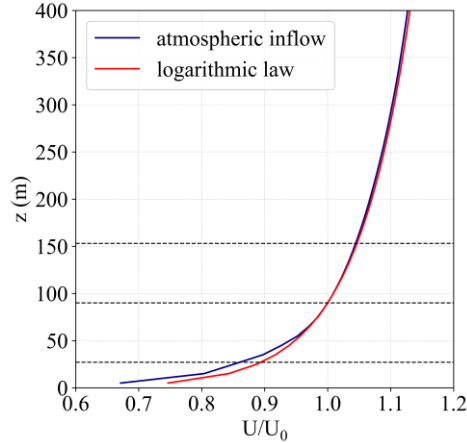
RESULTS AND DISCUSSIONS

ABL wind field

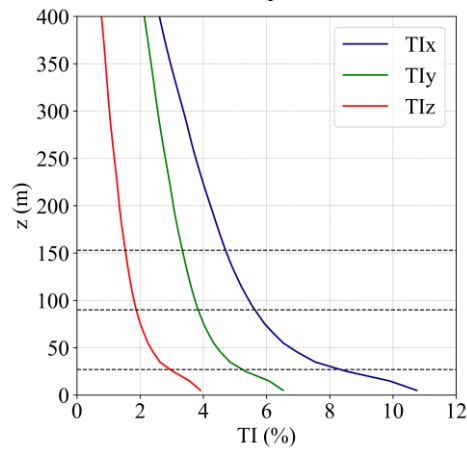
The ABL wind field is simulated by the LES with sufficient simulation duration for the inflow wind condition of FOWT, Figure 7 shows the time-averaged profiles, including the wind speed and turbulence intensity. The turbulence intensity is calculated by (Ning and Wan, 2019; Xu et al., 2023):

$$TI_i(z) = \frac{\sqrt{\overline{(U_i(z) - \bar{U}_i(z))^2}}}{U_0} \quad (6)$$

where, the overbar is time average, $U_i(z)$ is the wind speed of the height of z ($i = x, y, z$), and U_0 is the rated wind velocity of 11.4m/s. The wind speed at hub height is 11.4m/s, and the wind profile shows a good agreement with the logarithmic law, indicating that the desired atmosphere inflow is reproduced. The turbulence intensity decreases with height, and its component of x-axis is more significant than that of the other two directions. Specifically, the three components of turbulence intensity at hub height are 5.78, 3.82 and 1.85, respectively.



(a) Wind speed



(b) Turbulence intensity

Figure 7. Time-averaged profiles of the ABL wind field simulated by the LES. Three dashed lines denote the top, middle and bottom of the rotor area, respectively.

Rotor power

Figure 8 shows the rotor power of the FOWT for the two yaw operation scenarios, as well as the rotor power of non-yaw situation. We can clearly observe the change of rotor power with the period of incident regular wave. What's more, the insufficient rotor power between time instants of 400s and 450s is visible, which may be attributed to the large-scale low-speed airflow in the ABL wind field. For the non-yaw scenario, the influence of incident wave on rotor power is not significant compared to that of the yawed situations, because the blade pitch controller is active to limit the generation of rotor power. When the yaw angle is 15°, the rotor power is slightly decreased due to the decreased windward sweep area of rotor caused by yaw operation, and the decrease of rotor power is more obvious at 30° yaw angle.

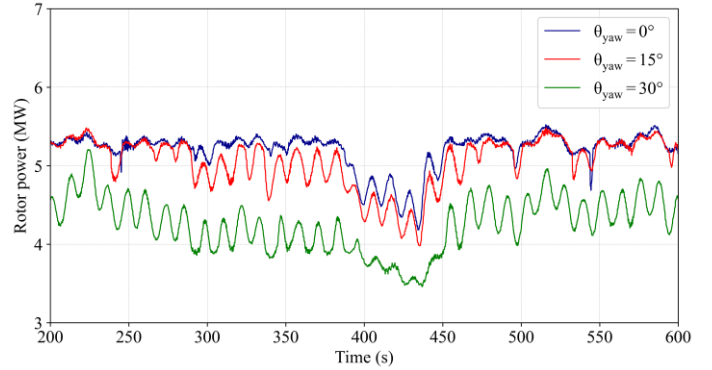


Figure 8. Rotor power of the FOWT.

In addition to the time histories, we present a quantitative analysis of the rotor power of the yawed FOWT, as illustrated in Table 3. From the statistics of rotor power, it is concluded that the values of maximum, minimum, mean and root mean square are decreased when the wind turbine is in the yaw operation, indicating that yaw of wind turbine can reduce its rotor power. However, for the root mean square of rotor power, the reduced value is 0.13MW when the yaw angle is 15° compared to that of non-yaw situation, which is significantly less than the reduced rotor power of 0.94MW at 30° yaw angle. This indicates that the decrease of rotor power with increase of yaw angle shows a non-linear characteristic. What's more, the standard deviation of rotor power is enhanced by the increase of yaw angle.

Table 3. Statistics of rotor power of the FOWT.

Case	Rotor power (MW)				
	Max	Min	Mean	Rms	Std
$\theta_{yaw} = 0^\circ$	5.52	4.18	5.20	5.20	0.24
$\theta_{yaw} = 15^\circ$	5.48	3.98	5.06	5.07	0.32
$\theta_{yaw} = 30^\circ$	5.20	3.46	4.26	4.27	0.35

Rotor thrust

Compared to the rotor power, the rotor thrust is also an important parameter for the FOWT. We show the time histories of rotor thrust of the yawed FOWT in Figure 9. As expected, the rotor thrust of the FOWT changes with the period of incident regular wave, which is consistent with the previous analysis of rotor power. However, we observe an interesting phenomenon that the rotor thrust of 15° yaw angle is larger than that of non-yaw scenario sometimes, which is inconsistent with the previous conclusion that the yaw operation of wind turbine can reduce its rotor power. According to the definition of NREL 5MW wind turbine

(Jonkman et al., 2009), its rotor thrust increases first and then decreases with the increase of wind speed, and the wind speed corresponding to maximum rotor thrust is slightly less than 11.4m/s. The yaw operation of wind turbine can be equivalent to the reduction of inflow wind speed with the same rotor windward sweep area of non-yaw scenario. Consequently, the rotor thrust with a small yaw angle (i.e., 15°) maybe larger than that of non-yaw situation when the wind turbine operates under 11.4m/s wind speed. But if the yaw angle is larger, the rotor thrust of FOWT is less than the value of non-yaw scenario, as shown in the rotor thrust of 30° yaw angle.

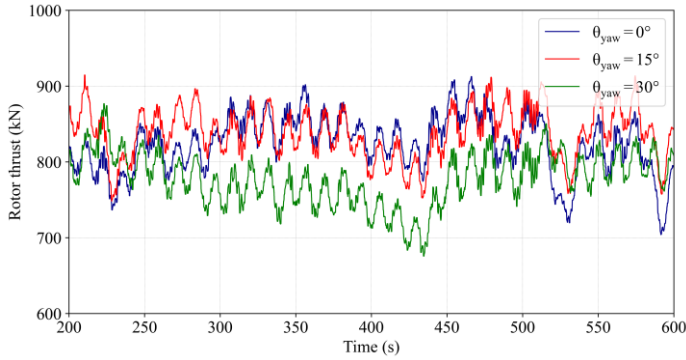


Figure 9. Rotor thrust of the FOWT.

Table 4 illustrates the statistics of rotor thrust of the FOWT. As expected, the maximum, minimum, mean and root mean square of rotor powers under 15° yaw angle are larger than that of non-yaw scenario, which is in line with previous qualitative analysis of rotor power. Specifically, the root mean square of rotor thrust of 15° yaw angle is 838.8kN, which is a slightly enhanced value than 824.8kN of non-yaw operation. When the yaw angle is 30°, the above four statistics are decreased because of the significantly reduced windward sweep area of turbine rotor. A conclusion is drawn that the rotor thrust of yaw FOWT is not decreased with increase of yaw angle always compared to the non-yaw scenario, instead, the rotor thrust is maximum under a small yaw angle (i.e., 15°).

Table 4. Statistics of rotor thrust of the FOWT.

Case	Rotor thrust (kN)				
	Max	Min	Mean	Rms	Std
$\theta_{yaw} = 0^\circ$	912.5	704.1	823.9	824.8	38.0
$\theta_{yaw} = 15^\circ$	914.5	748.3	838.1	838.8	33.6
$\theta_{yaw} = 30^\circ$	876.7	675.7	778.0	778.8	34.9

Platform motions

Figure 10 illustrates the six degree-of-freedom motions of the floating platform for the three cases. The regular variations of platform surge, heave and pitch induced by incident regular wave are clearly visible. Specifically, there is no difference for the platform heave motion between the two yaw scenarios and non-yaw scenario. The platform surface motion of 15° yaw angle is sometimes larger than that of non-yaw condition, and sometimes less than that of non-yaw condition, which is consistent with the previous analysis of rotor thrust. The rotor thrust of 15° yaw angle is slightly larger than the value of non-yaw scenario and streamwise component of 15° yaw angle is a value slightly less than 1. Consequently, the streamwise component of rotor thrust of 15° yaw angle is close to the rotor thrust of non-yaw scenario, leading to the small

difference of platform surge motion between the two situations. However, when the yaw angle increases to 30°, a significant decrease of platform surge motion is visualized compared to the platform surge motion of non-yaw operation of wind turbine. The similar conclusion can be concluded for platform pitch motion.

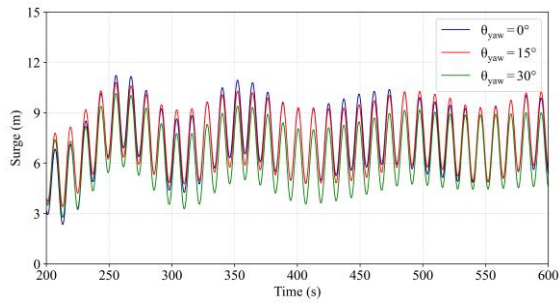
With respect to the other three platform motions, i.e., sway, roll, yaw, the hydrodynamic responses of floating platform increase with the increase of yaw angle of wind turbine. When the wind turbine operates in non-yaw condition, the three platform motions are close to 0, especially for the platform sway motion. However, if the wind turbine operates with a yaw angle, the sway motion of floating platform is enhanced by the crosswise component of rotor thrust of wind turbine, as shown in Figure 10(b). the platform sway motion of 30° yaw angle of wind turbine oscillates at 5m, and this value is reduced to 3m when the yaw angle decreases to 15°. For the platform roll and pitch motions, the distinct differences of the two yaw scenarios and non-yaw situation are not observed.

Wind turbine wake

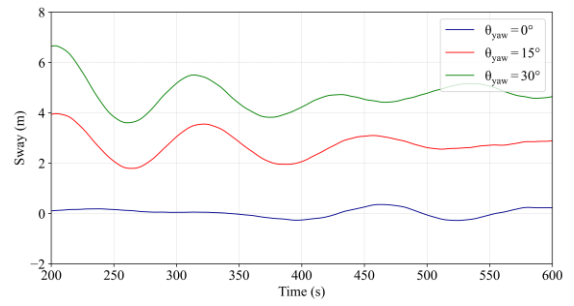
Figure 11 shows the time-averaged streamwise velocity contours at hub height level of FOWT, note that the contours are averaged using the data of last 400s. The wind turbine wake with significant velocity deficit is clearly visible, and the wake expansion is also clear when the wake travels downstream. Compared to the non-yaw scenario, the wake of wind turbine under 15° yaw angle deflects to right side when the sight towards downstream, and the deflection is enhanced with increase of yaw angle. In addition, we observe a faster wake recovery in yaw condition compared to that of non-yaw scenario. The wake of wind turbine under non-yaw operation is significant visible at downstream 10D, whereas this distance is reduced to downstream 9D and 7D when the yaw angles are 15° and 30°, respectively. A possible reason maybe that the mixing between outside ambient flow field and wind turbine wake is promoted by the crosswise component of velocity induced by yaw operation of wind turbine.

Figure 12 shows the wake center at hub height level for the three cases, with the aim of providing a quantitative insight on the effect of yaw angle on wind turbine wake. Note that the wake center is determined by using the Gauss fitting function. As expected, the wake center of non-yaw scenario closes to initial rotor center. For the situations of yaw operation of wind turbine, the wake center deflects away from the initial rotor center, and the deflection is enhanced with larger yaw angle. For instance, the wake centers of 15° and 30° yaw angles at downstream 7D are approximately -0.2D and -0.3D, respectively. In addition, the wake deflection between downstream 4D and 6D are significant than that of further downstream distance, which can be attributed to the gradually weak effect of crosswise component of velocity on wake deflection when the wake travels downstream.

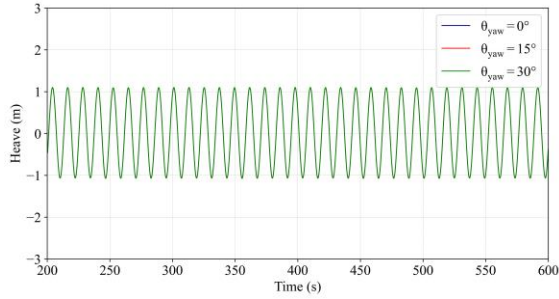
Figure 13 shows the time-averaged streamwise velocity contours of vertical plane at different downstream distances of FOWT. As shown, the wind velocity near bottom is lower than that of upper position, which is caused by the friction of sea surface and numerically implemented by surface stress model. For the non-yaw scenario, the wake expansion and wake recovery are significantly observed. In line with previous analysis of velocity contours at hub height level, the wake recovery under yaw angle is faster, and the wake recovery of 30° yaw angle is more significant than that of 15° yaw angle. In addition to wake recovery, the yaw operation of wind turbine leads to wind turbine wake far away from the initial position of wind turbine rotor, which is beneficial for the inflow wind condition and power generation of downstream wind turbine. Consequently, the yaw control by forcing upstream wind turbine to operate under a yaw angle maybe a potential technique to improve power generation of wind farm (Wei et al., 2021).



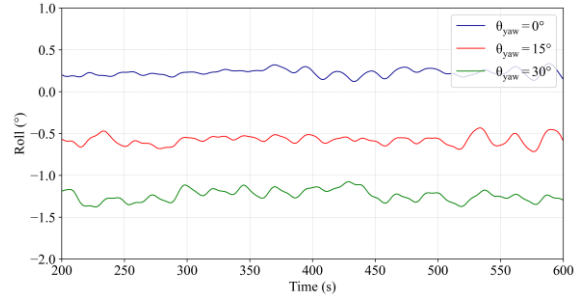
(a) Surge



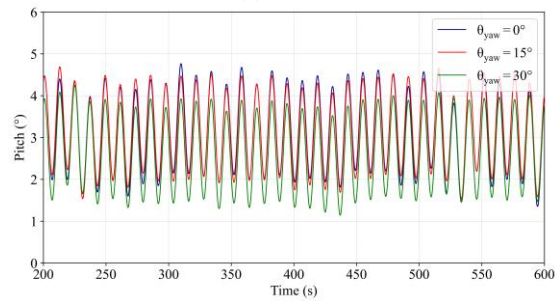
(b) Sway



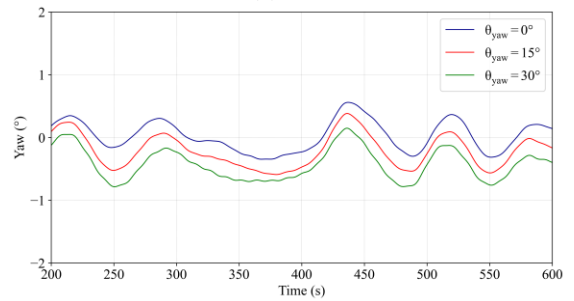
(c) Heave



(d) Roll

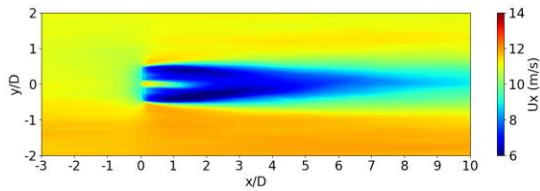


(e) Pitch

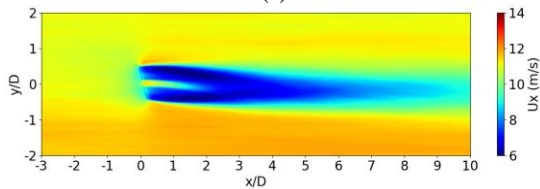


(f) Yaw

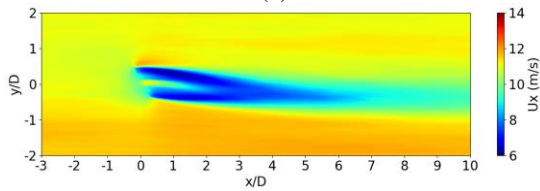
Figure 10. Platform motions of the FOWT.



(a)



(b)



(c)

Figure 11 Time-averaged streamwise velocity contours at hub height level of FOWT

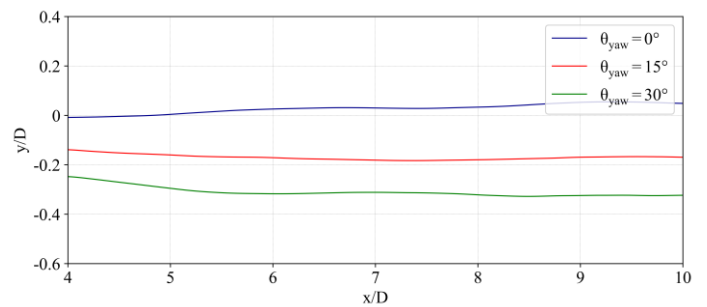


Figure 12. Wake center at hub height level of FOWT.

CONCLUSIONS

In this paper, we present numerical study of a yaw FOWT immersed in ABL wind field. The FOWT model is composed of NREL 5MW wind turbine and OC4 DeepCWind semi-submersible floating platform, and the ABL wind field is simulated and generated by the LES with sufficient simulation duration. The aero-hydro-moor-servo dynamics of FOWT is solved by NREL FAST code. Two yaw angles of 15° and 30° of wind turbine are performed, and the results of aerodynamics, hydrodynamics and wake characteristics are compared and analyzed with that of the non-yaw scenario.

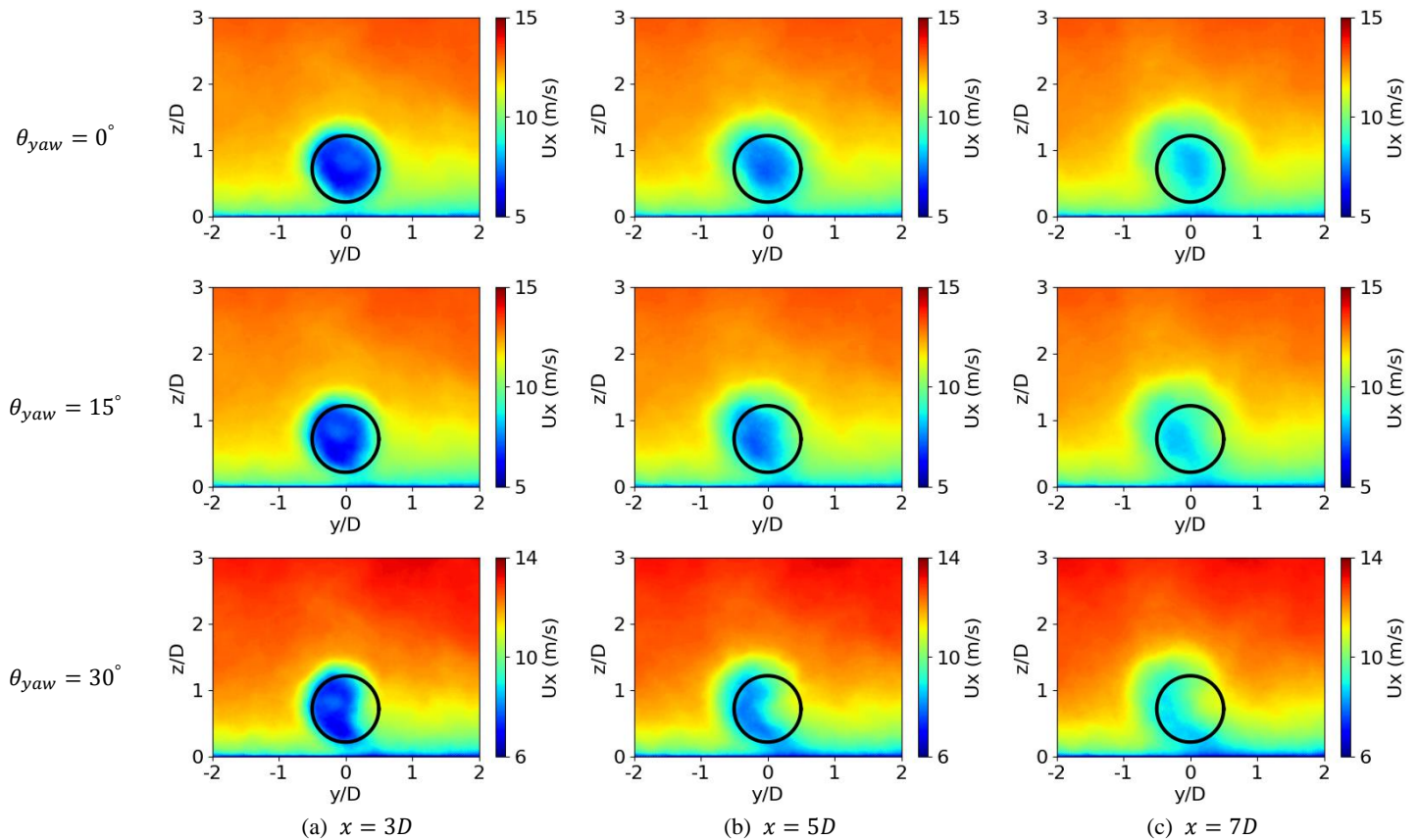


Figure 13. Time-averaged streamwise velocity contours of vertical plane at different downstream distances of FOWT. Rows denote the contours of different scenarios, and columns denote downstream 3D, 5D and 7D, respectively. Blade circle is the initial position of wind turbine rotor.

It is concluded that the rotor power of FOWT decreases with increase of yaw angle compared to that of non-yaw scenario. However, the rotor thrust of 15° yaw angle is 838.8kN, which is a slightly enhanced value compared to 824.8kN of non-yaw situation. Due to the significantly decreased rotor thrust, the platform surge motion and pitch motion of 30° yaw angle is less than that of non-yaw scenario, whereas the two platform motions of 15° yaw angle is close to that of non-yaw scenario because the rotor thrust is slightly increased and streamwise component of 15° yaw angle is a value slightly less than 1. The sway motion of floating platform is enhanced by the crosswise component of rotor thrust of wind turbine, consequently, the platform sway motion increase with the increase of yaw angle.

For wake characteristics of wind turbine wake, the wake recovery and wake expansion are clearly visible when the wake travels downstream. The faster wake recovery with increase of yaw angle is observed, specifically, the wake under non-yaw operation is significant visible at downstream 10D, whereas this distance is reduced to downstream 9D and 7D when the yaw angles are 15° and 30°, respectively. What's more, the wake center deflection is more significant with the increase of yaw angle, which is beneficial for the inflow wind condition and power generation of downstream wind turbine.

ACKNOWLEDGEMENTS

This work was supported by the National Natural Science Foundation of China (52131102), and the National Key Research and Development Program of China (2019YFB1704200), to which the authors are most grateful.

REFERENCES

- Churchfield M J, Lee S, Michalakes J, et al (2012a). "A numerical study of the effects of atmospheric and wake turbulence on wind turbine dynamics," *Journal of turbulence*, (13): N14.
- Churchfield M, Lee S and Moriarty P (2012b). "Overview of the simulator for wind farm application (SOWFA)," National Renewable Energy Lab. (NREL), Golden, CO (United States).
- Cheng P, Huang Y and Wan D (2019). "A numerical model for fully coupled aero-hydrodynamic analysis of floating offshore wind turbine," *Ocean Engineering*, 173: 183-196.
- Chanprasert W, Sharma RN, Cater JE, et al (2022). "Large Eddy Simulation of wind turbine fatigue loading and yaw dynamics induced by wake turbulence," *Renewable Energy*, 190: 208-222.
- Doubrawa P, Churchfield MJ, Godvik M, et al (2019). "Load response of a floating wind turbine to turbulent atmospheric flow," *Applied Energy*, 242: 1588-1599.
- Jasak H, Jemcov A and Tukovic Z (2007). "OpenFOAM: A C++ library for complex physics simulations," *Proceedings of the international workshop on coupled methods in numerical dynamics*. IUC Dubrovnik Croatia, 1000: 1-20.
- Huang Y and Wan D (2019). "Investigation of interference effects between wind turbine and spar-type floating platform under combined wind-wave excitation," *Sustainability*, 12(1): 246.
- Huang Y, Wan D and Hu C (2021). "Numerical analysis of aero-hydrodynamic responses of floating offshore wind turbine considering blade deformation," *Proceedings of the 31st International Ocean and Polar Engineering Conference*, June 20-25, 2021.

- Jonkman JM and Buhl ML (2005). FAST user's guide. National Renewable Energy Laboratory Golden, CO, USA.
- Jonkman J, Butterfield S, Musial W, et al (2009). "Definition of a 5-MW reference wind turbine for offshore system development," National Renewable Energy Lab. (NREL), Golden, CO (United States).
- Johlas HM, Martinez-Tossas LA, Churchfield M J, et al (2021). "Floating platform effects on power generation in spar and semisubmersible wind turbines," *Wind Energy*, 24(8): 901-916.
- Li L, Liu Y, Yuan Z, et al (2018). "Wind field effect on the power generation and aerodynamic performance of offshore floating wind turbines," *Energy*, 157: 379-390.
- Li Y, Huang X, Tee KF, et al (2022). "Comparative study of onshore and offshore wind characteristics and wind energy potentials: A case study for southeast coastal region of China," *Sustainable Energy Technologies and Assessments*, 39: 100711.
- Ning, X, and Wan, D (2019). "LES Study of Wake Meandering in Different Atmospheric Stabilities and Its Effects on Wind Turbine Aerodynamics," *Sustainability*, 11(24), 6939.
- NREL (2022). "FAST v8," Available online: <https://www.nrel.gov/wind/nwtc/fastv8.html/> (accessed on 26 December 2022).
- Porté-Agel F, Bastankhah M and Shamsoddin S (2020). "Wind-turbine and wind-farm flows: a review," *Boundary-Layer Meteorology*, 174(1): 1-59.
- Robertson A, Jonkman J, Masciola M, et al (2014). "Definition of the semisubmersible floating system for phase II of OC4," National Renewable Energy Lab. (NREL), Golden, CO (United States).
- Rohrig K, Berkhout V, Callies D, et al (2019). "Powering the 21st century by wind energy-Options, facts, figures," *Applied Physics Reviews*, 6(3): 031303.
- Ramachandran RC, Desmond C, Judge F, et al (2022). "Floating wind turbines: marine operations challenges and opportunities," *Wind Energy Science*, 7(2): 903-924.
- Smagorinsky J (1963). "General circulation experiments with the primitive equations: I. The basic experiment," *Monthly weather review*, 91(3): 99-164.
- Schumann U (1975). "Subgrid scale model for finite-difference simulations of turbulent flows in plane channels and annuli," *Journal of Computational Physics*, 18(4): 376-404.
- Sorensen JN and Shen WZ (2002). "Numerical modeling of wind turbine wakes," *Journal of Fluids Engineering*, 124(2): 393-399.
- Troldborg N, Sørensen JN and Mikkelsen R (2007). "Actuator line simulation of wake of wind turbine operating in turbulent inflow," *Proceedings of the Journal of physics: conference series*, IOP Publishing, 75(1): 012063.
- Troldborg N (2009). "Actuator line modeling of wind turbine wakes," PhD Thesis, Technical University of Denmark, Lyngby, Denmark.
- Tran TT and Kim DH (2016). "Fully coupled aero-hydrodynamic analysis of a semi-submersible FOWT using a dynamic fluid body interaction approach," *Renewable Energy*, 92: 244-261.
- Wei D, Zhao W, Wan D, et al (2021). "A new method for simulating multiple wind turbine wakes under yawed conditions," *Ocean Engineering*, 239: 109832.
- Xu S, Xue Y, Zhao W, et al (2022). "A Review of High-Fidelity Computational Fluid Dynamics for Floating Offshore Wind Turbines," *Journal of Marine Science and Engineering*, 10(10): 1357.
- Xu S, Wang N, Zhuang T, et al (2023). "Large Eddy Simulations of Wake Flows Around a Floating Offshore Wind Turbine Under Complex Atmospheric Inflows," *International Journal of Offshore and Polar Engineering*, 33(01): 1-9.
- Zhang Y and Kim B (2018). "A Fully Coupled Computational Fluid Dynamics Method for Analysis of Semi-Submersible Floating Offshore Wind Turbines Under Wind-Wave Excitation Conditions Based on OC5 Data," *Applied Sciences*, 8(11): 2314.
- Zhou Y, Xiao Q, Liu Y, et al (2022). "Exploring inflow wind condition on floating offshore wind turbine aerodynamic characterisation and platform motion prediction using blade resolved CFD simulation," *Renewable Energy*, 182: 1060-1079.